http://dx.doi.org/10.1109/icra.2018.8460515

# Vision-based Global Localization using Ceiling Space Density

Arthur Ribacki[1], Vitor A. M. Jorge[2], Mathias Mantelli[1], Renan Maffei[1] and Edson Prestes[1]

***Abstract*— Service robots are becoming a reality across homes. Still, the range of applications supported by such robots remains tied to their ability to self-localize in the environment. Man-made constructions often have a documented blueprint which can be used as input information for robot localization and smart home applications. However, home environments commonly include movable objects and furniture, which can make localization a complicated task, especially for forward-facing horizontal rangefinders. In this paper, we present a new and effective global localization approach for home environments which adapts the notion of free space density to a camera pointing to the ceiling. We exploit the available blueprint information, as well as evidence that ceiling vision can provide robust localization information, even in the presence of occlusions. We perform real-world experiments using a robotic vacuum cleaner equipped with an upward-facing camera in two different apartments across multiple trajectories and compare the proposed method with competing approaches. Our solution shows superior localization results using maps where neither furniture or movable objects are not modeled.**

## I. INTRODUCTION

The ability to estimate the robot's pose relative to its environment is a key problem in mobile robotics [1]. This work focuses particularly on the global localization problem, where the robot should self-localize on a reference map without any prior knowledge of its current pose. Over the last decades many solutions were proposed, differing in the structure of the reference map, the required sensors, and the method used for pose estimation.

Maps can be generated using simultaneous localization and mapping (SLAM) approaches [2]–[4]. Alternatively, they can be manually constructed, with techniques varying from hand-drawn approximations [5] to detailed 3D models [6], [7], or represented by a set of images previously captured at known locations [8]–[10]. Furthermore, as service robots get increasingly integrated with smart home systems, new resources become readily available. For instance, a good user interface for such system should already include a representation of the environment, e.g. a blueprint, pointing the location of connected smart devices [11]. Besides, blueprints are widely available in the case of man-made construction and even mandatory in some countries due to regulatory legislation. Therefore, using blueprints for global localization is practical, efficient and enables a wider variety of applications inside smart systems.

[1]Institute of Informatics, UFRGS, Porto Alegre, Brazil avribacki, rqmaffei, mfmantelli, prestes@inf.ufrgs.br

[2]Autonomous System Lab, Faculty of Informatics, PUC-RS, Porto Alegre, Brazil vitor.jorge@cwldalgorithm.com

Special thanks for the Eldorado Institute, CAPES and CNPq for the support and founding.

There are two main approaches for global localization: direct pose estimation from a single measurement and recursive estimation based on continuous observation. The former includes landmark-based methods where the position of matched features is used to estimate the robot's actual pose relying on fitting algorithms [2]–[4]. Similarly, image-retrieval methods can be employed, where a training set of images captured at known poses are used for estimation [8]–[10]. Those methods can quickly estimate the global position from a single measurement but are limited by perceptual aliasing and will fail in environments with periodical structures [12]. To overcome this limitation, probabilistic approaches, such as the Monte Carlo Localization (MCL) [13], have been widely employed [1], [6], [14], [15]. As the robot moves, new observations are used to recursively refine the estimated pose.

In this work, we propose an effective ceiling vision-based localization strategy for indoor service robots equipped with an upward facing camera. The solution is an extension of the MCL implementation proposed in [16], which uses the Free Space Density (FSD) observation model. Instead of using a laser rangefinder to reconstruct the robot surroundings to estimate the local density, we extract the ceiling boundaries from the currently perceived image. The approach does not require any information about furniture position, only a bare blueprint of the walls.

We performed real-world experiments using a Neato XV-12 vacuum cleaner, equipped with a wide-angle monocular camera in two different apartments across multiple trajectories. For the first scenario, the blueprint is hand-made, while for the second it is extracted directly from its construction plan. They demonstrate the feasibility and effectiveness of the proposed solution even in the presence of temporary occlusions like tables or consistent differences like high furniture.

## II. RELATED WORK

One of the earliest MCL works by Dellaert et al. [13] was also based on ceiling view. The map is a mosaic of a museum's ceiling constructed from previous explorations and the observation model is a single brightness measurement of the ceiling directly above the robot. It demonstrates that little sensing is required for MCL convergence. Nevertheless, the abundance and consistency of lights present in a museum cannot be expected in home environments and, as evidenced by our experiments, the approach is not so effective in such environments.

Since then, many global localization approaches have benefited from the robustness of using ceiling vision. In the

work of Jeong et al. [3], a map of 3D ceiling landmarks is reconstructed using an EKF-based SLAM. Relocation is later performed by matching the current image features to the reference map using Hough clustering. Hwang et al. [2] extend this approach by using arbitrarily-shaped ceiling features and significantly reduce the number of candidate positions. However, indistinguishable features commonly found in ceilings can hinder data association, therefore limiting their use [17].

From the explored ceiling features, Choi et al. [18] is the closest to our approach. It also segments the ceiling boundaries from camera images, but instead of considering the free space area, the boundaries themselves are used as features for mapping using an EKF-SLAM. Unfortunately, it focuses on SLAM and does not tackle global localization.

Another line of research explores alternatives to SLAM-based maps. Ho et al. [6] use a 3D laser scanner coupled with a camera to manually create a detailed 3D model of the environment. An appearance-based model is derived from it by simulating omnidirectional views every 0.5 meters. Global localization is later performed using a particle filter where the weight of each particle is computed using Haar wavelets features as similarity measurements. Mason et al. [15] uses a similar 3D laser with camera setup, but the constructed map is stored as a 3D textured occupancy grid. They also uses a particle filter, but simulated views are created on demand considering each particle pose and the $L_2$ norm of their difference is used as weight.

In Kitanov et al. [7], a metric 3D model is manually constructed using a professional computer graphics tool without requiring previously recorded images of the environment. Similarly to our approach, it relies only on the perceived geometric structure, i.e., lines that are detected on both rendered and captured images. However, they solve only pose tracking and their map creation is far more complex than the 2D blueprints used in our solution. Ramalingam et al. [19] follow a similar path for pose tracking in outdoor urban canyons. Instead of the ceiling, the skyline is extracted from upward omnidirectional images and matched against GPU generated skylines based on a coarse 3D model of the city.

## III. VISION-BASED LOCALIZATION ON BLUEPRINTS USING CEILING SPACE DENSITY

### A. The Map

A simplified blueprint image, containing only the walls and other relevant ceiling features, is used to initialize the reference occupancy grid [20]. Cells that are associated with pixels corresponding to walls are set as an obstacle while the remaining are set as free space. Doorways are set with low occupancy probability to delimit the correct ceiling boundaries while still allowing the robot to cross that area. Fig. 1 shows part of the blueprint and the resulting occupancy grid map used in one of the experiment scenarios.

One can note that neither furniture nor movable objects are represented in the resulting grid map. While furniture information could be useful, their position can change, compromising map accuracy.

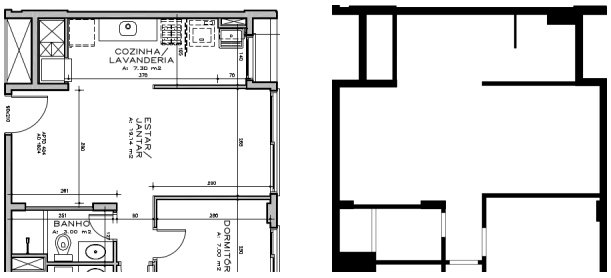


(a) (b)

Fig. 1: Blueprint (a) and generated occupancy grid (b).

### B. Ceiling Space Density

The core idea of this proposal is based on the Free Space Density (FSD) introduced by Maffei et al. [16] for global localization of robots equipped with a laser rangefinder. Instead of using the surrounding free space, we compute the Ceiling Space Density (CSD) as delimited by the ceiling boundaries detected using an upward facing camera.

One of the advantages of using space density is that, since the result is orientation independent, it can be precomputed for each cell of the reference map and stored as a single value per cell, allowing the simulated observation at each position to be readily accessible.

The CSD $\Psi$ of a region centered at cell $\mathbf{m}_0$ can be computed using a kernel density estimate defined as follows

$$\Psi(\mathbf{m}_0) = \sum_{\mathbf{m}_i} s(\mathbf{m}_i, \mathbf{m}_0) K(||\mathbf{m}_i - \mathbf{m}_0||) \qquad (1)$$

where $K(.)$ is a kernel profile[1], $\mathbf{m}_i$ are the cells limited by the kernel radius and

$$s(\mathbf{m}_i, \mathbf{m}_0) = \begin{cases} 1 & \text{, if } \mathbf{m}_i \text{ is } \textit{visible} \text{ from } \mathbf{m}_0 \\ 0 & \text{, otherwise} \end{cases} \qquad (2)$$

This formulation diverges from the original FSD proposal where $s(\mathbf{m}_i, \mathbf{m}_0)$ considers all the cells within the kernel radius that belongs to the free space connected to $\mathbf{m}_0$. In the example presented in Fig. 2b, FSD would also consider the red cells beyond the visible ones highlighted in green. This change was made since the ceiling can be occluded by walls, as seen in Fig. 2a.

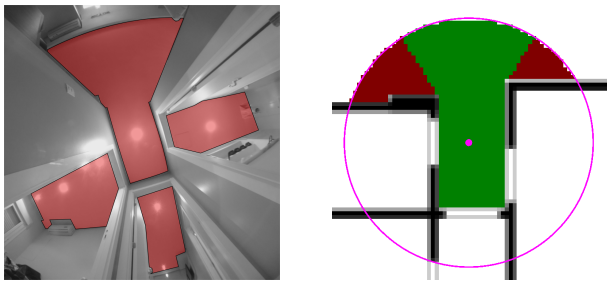

(a) (b)

Fig. 2: Ceiling view with considerable wall occlusion (a) and its global map position with overlayed kernel area (b).

[1]In this work we use a Gaussian kernel profile as defined in [16].

(a) (b) (c) (d)

Fig. 3: Steps to calculate CSD from a given frame: (a) original, (b) dewarped, (c) segmented ceiling, and (d) the resulting occupancy grid overlayed by the kernel.

### C. Ceiling Extraction

In order to compute the CSD from ceiling images, we first need to extract the ceiling boundaries. We use the method proposed by Choi et al. [18], described in Algorithm 1.

**Algorithm 1:** Ceiling segmentation

1 Blur the image for reducing noise.
2 Expand the ceiling part from the center of the image, until it reaches strong edges
3 Merge small blobs inside the ceiling part
4 If the ceiling part occupies more than $\Delta$ of the image, terminate the procedure. Otherwise, go back to 2

In [18], the value of $\Delta$ is set to 40% as their camera has a narrow field of view (FoV). To have correct CSD estimation, the FoV should be sufficiently large to cover, at least, the region occupied by the kernel. For this reason, a wide-angle lens with a wider FoV was used, which leads to smaller $\Delta$ values. In our case, the FoV was about 180° and $\Delta$ was set to 4%. Fig. 3a and b show respectively the original captured image and the result after perspective correction.

Once the ceiling is segmented (Fig. 3c), it is flipped vertically and horizontally, to convert between image and world coordinates, and rotated using the orientation estimated by odometry. This last step could be omitted since it is later nulled by computing the $\alpha_t^{robot}$ used in equation 5 as the difference between the gradient and odometry orientation. Nevertheless, the rotation was maintained to keep consistency with original FSD formulation. Finally, the resulting image is converted to an occupancy grid using a scale factor that is dependent on the camera intrinsic parameters and the cell size used on the reference map. The final map, overlaid by the corresponding kernel, can be seen in Fig. 3d.

Note that even if the ceiling is occluded by nearby objects, such as the table and chair shown in the left of Fig. 3a, the CSD is correctly estimated since there is no overlap between the kernel region and the occlusion. A smaller kernel means that the process is more robust against occlusions, but at the same time it can create large areas with homogeneous density that cause perception aliasing problems.

### D. Proposed global localization method

Monte Carlo Localization (MCL) is a recursive Bayes filter that estimates the posterior distribution of robot poses conditioned on sensor data [1]. The robot pose is represented by a set of weighted particles that approximates such distribution without imposing restrictions on its form, while, at the same time, efficiently tracking multiple hypotheses – a prerequisite for global localization. At each iteration, particles are updated according to the motion model and weighted based on the observation model.

In vision-based methods, the observation model should determine the likelihood of a particle to perceive the current camera image given its pose on the map. In our approach, this likelihood is achieved by comparing the CSD value at particle positions against the perceived CSD from the extracted ceiling. This means that after ceiling extraction and local CSD computation, the particle weighting boils down to a couple of scalar comparisons which is very efficient, even when using many particles.

The weight $w(\boldsymbol{p}_t^{[i]})$ for the $i$-th particle at step $t$ is computed using two factors: one based on the density estimates, $f_\Psi(\boldsymbol{p}_t^{[i]})$, and other based on orientation estimates, $f_\alpha(\boldsymbol{p}_t^{[i]})$.

$$w(\boldsymbol{p}_t^{[i]}) = f_\Psi(\boldsymbol{p}_t^{[i]}) \cdot f_\alpha(\boldsymbol{p}_t^{[i]}) \tag{3}$$

The first term represent the similarity between the observed CSD, $\Psi(\boldsymbol{m}_t^{robot})$, and the precomputed value at particle position, $\Psi(\boldsymbol{m}_t^{[i]})$,

$$f_\Psi(\boldsymbol{p}_t^{[i]}) = 1.0 - \frac{\min(\left|\Psi(\boldsymbol{m}_t^{robot}) - \Psi(\boldsymbol{m}_t^{[i]})\right|, \Delta_\Psi)}{\Delta_\Psi}, \tag{4}$$

where $\Delta_\Psi$ is the difference between the maximum and minimum CSD found in the reference map. Particles for which the observation error is greater than $\Delta_\Psi$, will have weight equal to zero and are later discarded.

Similarly to [16], the gradient of the scalar CSD field is used to estimate the likelihood of particles orientation. First, we compute the angle difference, $\alpha_t^{robot}$, between the robot orientation given by odometry and the gradient direction of the CSD field surrounding the robot. Likewise, we compute

the angle difference, $\alpha_t^{[i]}$, associated with the $i$-th particle using the CSD field of the reference map. The orientation weight is then given by the similarity between the two.

$$f_\alpha(\boldsymbol{p}_t^{[i]}) = 1.0 - \frac{\left|\alpha_t^{robot} - \alpha_t^{[i]}\right|}{\pi} \tag{5}$$

Unfortunately, this information becomes less reliable when the gradient direction changes abruptly and the orientation weight $f_\alpha(\boldsymbol{p}_t^{[i]})$ cannot be used in those cases. Due to the smooth nature of the novel density proposal, direction changes will be drastic mainly near low intensity gradient regions. When the perceived gradient intensity is smaller then a given threshold $\epsilon$, the orientation information is not considered, i.e. $f_\alpha(\boldsymbol{p}_t^{[i]}) = 1$.

## IV. EXPERIMENTAL RESULTS

To demonstrate the feasibility and effectiveness of our approach, we execute a sequence of global localization tasks, using a Neato-XV 12 robotic vacuum cleaner[2], coupled with a wide-angle lens camera pointing to the ceiling.

We compare the proposed approach (CSD) with the original MCL from Dellaert *et al.* [13], the original laser-based approach [16] (FSD), along with pure motion to evaluate the level of contribution of the observation step with respect to the overall uncertainty reduction.

All approaches were tested in two different scenarios, corresponding to two different apartments. For each, the robot is manually moved through three different trajectories (see Figs. 4a-b) while recording camera frames, odometry data, and laser readings. The final position of each run is manually measured relative to the walls, later converted to a global position in the map and used as ground-truth. The global localization is performed in real time, but the tests are repeated offline due to the probabilistic nature of the method. Each recorded path is executed 10 times and the results presented here are the mean of those executions. In all experiments, the number of particles is set to 10.000.

After each resampling step, we use the EM algorithm to estimate the mean and covariance of the particle's position as if they represented an unimodal 2D Gaussian distribution. The area within 2 standard deviations (95%) is then used as uncertainty measure and is represented as oriented ellipses in Fig. 5. Even if the distribution is multi-modal before convergence, this approach will result in high uncertainty and can be used to determine the convergence speed of the method. Note that convergence alone does not implicate successful operation and should be considered together with the final position error when determining localization effectiveness.

Prior to the execution of the experiments, the CSD and FSD fields of each environment were precomputed using available blueprints (see Figs. 4e-h). For both scenarios, a kernel radius of $1.6m$ provided a good balance between robustness and effectiveness. To execute Dellaert et al. [13], the mosaic from the ceiling of each apartment, Figs. 4c-d, were manually constructed using captured images. The structural

[2]Produced by Neato Robotics. https://www.neatorobotics.com/

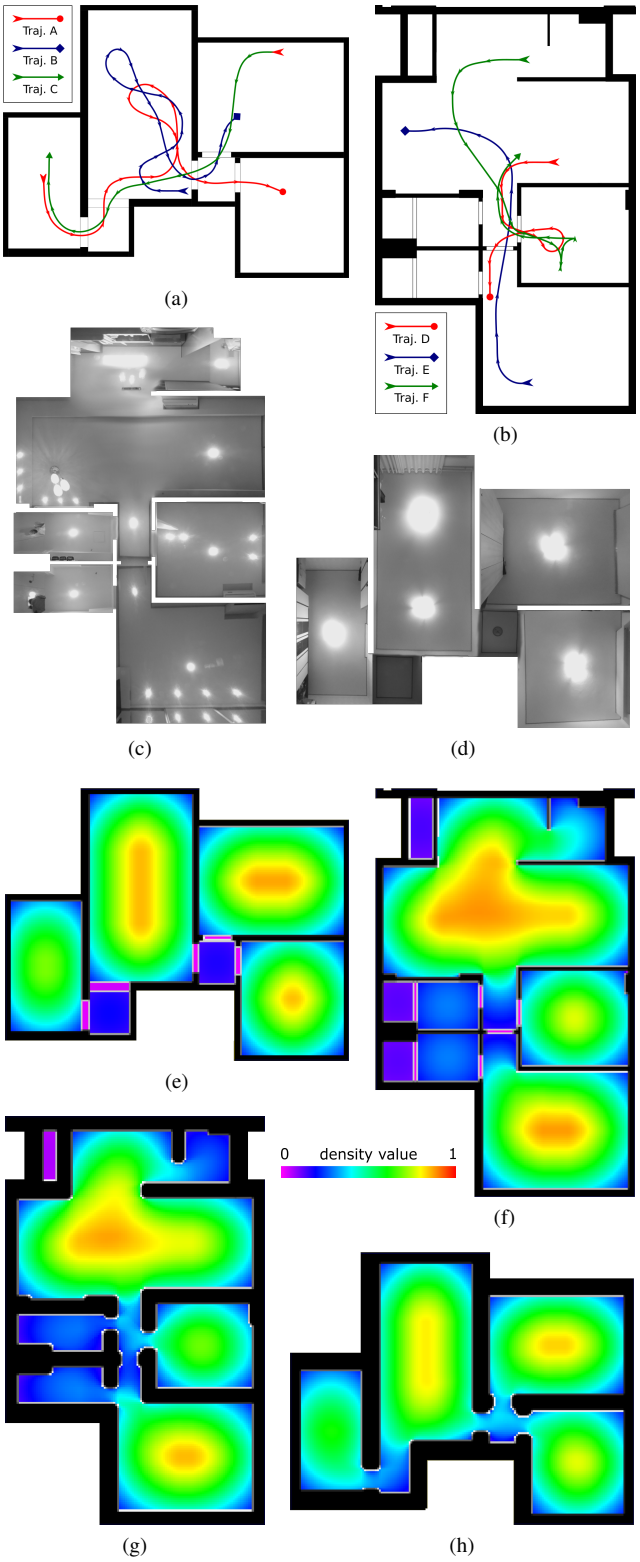


Fig. 4: Trajectories used in the experiments (a-b), ceiling mosaics used for Dellaert [13] (c-d) and precomputed density fields for CSD (e-f) and FSD [16] (g-h).

(a) Step 19 (b) Step 81

Fig. 5: Examples of particles distribution (red dots) during trajectory A. The mean position is represented by the yellow dot and the uncertainty by the surrounding ellipse.

information from the blueprints is also encoded in the mosaic by setting the walls as transparent pixels that the particles cannot go through.

### A. Results

Table I presents final localization results for pure motion, Dellaert et al. [13], original laser-based FSD [16] and proposed method (CSD). Results from the first apartment are shown in trajectories A-C, while the results for the second apartment are shown in trajectories D-F. The uncertainty of the particle filter, considering the average over the 10 runs, for each method and trajectory is displayed in Fig. 6.

| Trajectory lenght | | A $15.2m$ | B $12.9m$ | C $10.7m$ | D $9.1m$ | E $8.4m$ | F $12.2m$ |
|---|---|---|---|---|---|---|---|
| **Method** | | **Error** $(m)$ | | | | | |
| Motion | $\mu$ | 0.64 | - | - | - | - | 0.36 |
| | $\sigma$ | 0.06 | - | - | - | - | 0.08 |
| Dellaert [13] | $\mu$ | 0.62 | **0.24** | 0.96 | - | - | 0.48 |
| | $\sigma$ | 0.09 | 0.04 | 0.06 | - | - | 0.04 |
| FSD [16] | $\mu$ | - | - | - | 3.09 | 1.14 | 3.44 |
| | $\sigma$ | - | - | - | 1.40 | **0.08** | 0.06 |
| **CSD** | $\mu$ | **0.05** | 0.24 | **0.16** | **0.30** | **0.84** | **0.22** |
| | $\sigma$ | **0.02** | **0.02** | **0.02** | **0.02** | 0.10 | **0.03** |
| **Method** | | **Uncertainty** $(m^2)$ | | | | | |
| Motion | $\mu$ | 6.94 | 32.90 | 96.63 | 68.58 | 79.88 | 17.65 |
| | $\sigma$ | 1.13 | 2.02 | 25 | 4.11 | 5.57 | 2.78 |
| Dellaert [13] | $\mu$ | 7.07 | 0.99 | 2.02 | 75.05 | 70.91 | 2.11 |
| | $\sigma$ | 3.77 | 0.10 | 1.07 | 6.38 | 13.93 | 0.85 |
| FSD [16] | $\mu$ | 33.18 | 27.40 | 28.43 | 5.52 | **0.41** | 0.46 |
| | $\sigma$ | 36.44 | 39.49 | 24.97 | 15.13 | **0.15** | 0.07 |
| **CSD** | $\mu$ | **0.30** | **0.34** | **0.37** | **0.64** | 1.24 | **0.45** |
| | $\sigma$ | **0.02** | **0.05** | **0.01** | **0.02** | 0.18 | **0.03** |

TABLE I: Experiment Results. The final error was not calculated when the final uncertainty was greater than $20m^2$

Using an Intel Core 2 Duo clocked at 1.66GHz, the mean execution time for the perception step took about $94ms$, including image de-warping, ceiling segmentation, and CSD calculation. This time is independent of the number of particles: once the perceived CSD is computed, each particle weight resumes to few arithmetic operations. For the 10.000 particles used in the experiments, the mean update time was about $127ms$, including both weighting and resampling steps. As a comparison, the observation time using FSD with laser is about $4ms$, excluding local map reconstruction, and for Dellaert was $26ms$. Even though they are faster than the proposed method, their final error in the tested scenarios is generally much larger (considering only the cases that they converge to a solution), as we show next.

As seen in Table I, trajectory A presents the smallest final error for CSD and in fact, it is the only trajectory that finishes in a room where the ceiling matches the blueprint. All other final positions are in rooms with high furniture that blocks part of the ceiling. In trajectory E, the worst result, the final position is very close to the celling unevenness that crosses the large room of the second apartment, that can be seen in Fig. 4c but is not modeled in Fig. 4f-g. Even in the presence of such challenges, the proposed solution always converged, sometimes displaced by a constant factor due to such disparities. We could have added more information to the reference map to improve the results, but we wanted to test the limits of what is achievable using bare blueprints. This also demonstrates the robustness of the method and that the ceiling view is indeed a good approximation of the blueprint in real-world examples.

For trajectories B-E, pure motion never leads to convergence, while the proposed approach and Dellaert et al.'s [13] present superior results, discarding the possibility of motion as the only responsible for the convergence. However, note that CSD converges in all trajectories, while Dellaert et al. [13] diverges in trajectories D-E. Besides, apart from trajectory B, CSD presents superior means and standard deviations, for both error and uncertainty, in all scenarios. Convergence and the transition from global localization to tracking can be clearly observed in Figs 6 a-f, where in all trajectories but B, CSD converges faster. Trajectory B was specially designed for Dellaert et al. [13], passing under the two lights of the central room. Still, we highlight that lights are normally over tables or other furniture that require illumination and, in fact, for trajectory B we had to displace the dinning table, so the robot could pass under the light. Also, not all lights will be turned on all the time, which can also lead to incorrect associations.

Regarding FSD, it diverged and the filter was restarted several times in A-C and F, while in D it diverged and never recovered, converging only in E. This is expected since FSD relies on a forward-facing laser range finder and no furniture is shown in the map. Even if the comparison might be unfair, it helps illustrate the limitations of methods that require more detailed maps for global localization. To achieve an improved performance with FSD, another map, considering every single piece of furniture in the environment, should be used – which is less practical than mapping only the walls.

## V. CONCLUSION

In this paper, we present a novel vision-based global localization approach for indoor service robots. Experimental results using a robotic vacuum cleaner in different scenarios demonstrate the robustness and feasibility of the method when compared to competing approaches. The proposed method takes advantage of the notion of free space density, adapted to data obtained from a camera pointing to the ceiling. The method does not require any precomputed 3D

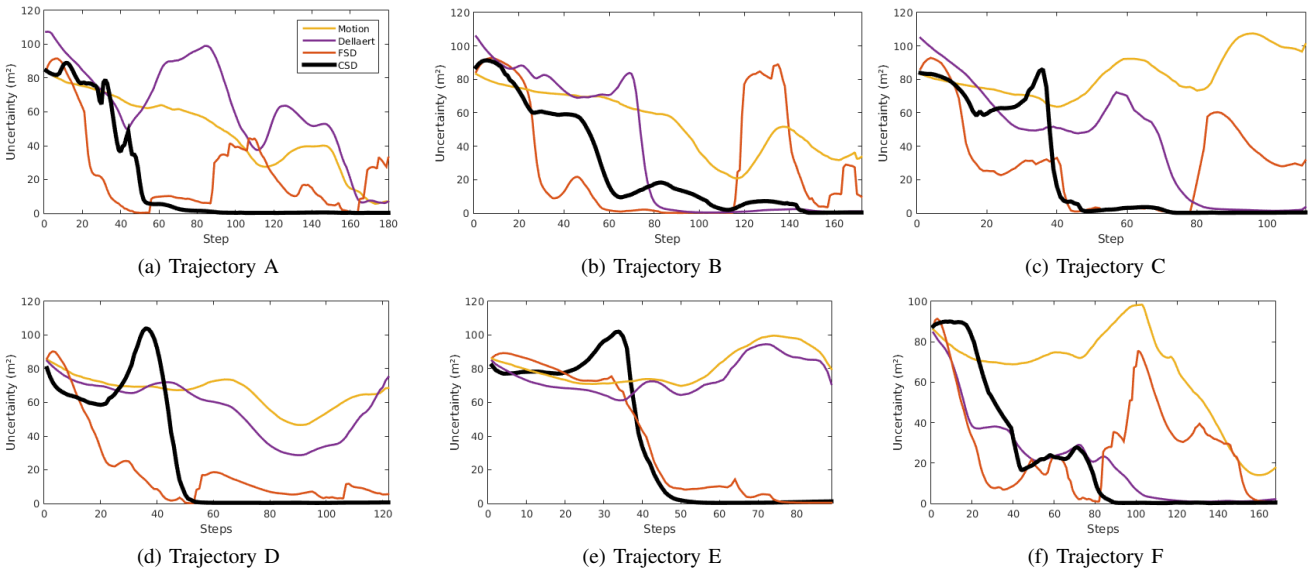


(a) Trajectory A (b) Trajectory B (c) Trajectory C

(d) Trajectory D (e) Trajectory E (f) Trajectory F

Fig. 6: Mean of uncertainty evolution for each trajectory.

space model, which is fundamental for many approaches relying on feature matching or simulated view generation, as mentioned in Section II. It also does not require the position of existing furniture, instead, it works only with bare blueprints.

Currently, the proposed approach requires uniform ceiling colors and may not work if a large part of the ceiling view is occluded for a long period during the localization process – such limitation must be taken into consideration mainly if such occlusions happen before the tracking phase. However, we highlight that during the tests the robot passed nearby tables and other objects, which momentarily caused large occlusions in the robot's view, but the algorithm still presented good results.

In the future, we plan to study different forms of ceiling segmentation, focusing on non-uniform ceiling scenarios to increase the spectrum of environments where the approach can be used. In addition, we plan to test and combine different kernel density estimates, to determine if the convergence times of the algorithm can be improved even further.

## REFERENCES


[1] S. Thrun, D. Fox, W. Burgard, and F. Dellaert, "Robust monte carlo localization for mobile robots," *Artificial Intelligence*, vol. 128, no. 1-2, pp. 99–141, 2001.

[2] S.-Y. Hwang and J.-B. Song, "Monocular vision-based global localization using position and orientation of ceiling features," in *Proc. of 2013 IEEE ICRA*. IEEE, May 2013, pp. 3785–3790.

[3] W. Jeong and K. M. Lee, "CV-SLAM: a new ceiling vision-based SLAM technique," in *Proc. of 2005 IEEE/RSJ IROS*. IEEE, 2005, pp. 3195–3200.

[4] M. Tomono, "3D localization based on visual odometry and landmark recognition using image edge points," in *Proc. of 2010 IEEE/RSJ IROS*. IEEE, Oct. 2010, pp. 5953–5959.

[5] B. Behzadian, P. Agarwal, W. Burgard, and G. D. Tipaldi, "Monte carlo localization in hand-drawn maps," in *Proc. of 2015 IEEE/RSJ IROS*. IEEE, Sep. 2015, pp. 4291–4296.

[6] N. Ho and R. Jarvis, "Vision based global localisation using a 3D environmental model created by a laser range scanner," in *Proc. of 2008 IEEE/RSJ IROS*. IEEE, Sep. 2008, pp. 2964–2969.

[7] A. Kitanov, S. Bisevac, and I. Petrovic, "Mobile robot self-localization in complex indoor environments using monocular vision and 3D model," in *Proc. of 2007 IEEE/ASME AIM*. IEEE, 2007, pp. 1–6.

[8] M. Jogan and A. Leonardis, "Robust localization using an omnidirectional appearance-based subspace model of environment," *Robotics and Autonomous Systems*, vol. 45, no. 1, pp. 51–72, Oct. 2003.

[9] J. Wang, R. Cipolla, and H. Zha, "Vision-based global localization using a visual vocabulary," in *Proc. of 2005 IEEE ICRA*. IEEE, 2005, pp. 4230–4235.

[10] S. Yoon, W. Han, S. Min, and K. Roh, "Global localization of mobile robot using omni-directional image correlation," in *Advances in Image and Video Technology*, ser. Lecture Notes in Computer Science, L.-W. Chang and W.-N. Lie, Eds., 2006, vol. 4319, pp. 433–441.

[11] J. Lu and K. Whitehouse, *Smart Blueprints: Automatically Generated Maps of Homes and the Devices Within Them*. Springer Berlin Heidelberg, 2012, vol. 7319, ch. 9, pp. 125–142.

[12] E. Menegatti, M. Zoccarato, E. Pagello, and H. Ishiguro, "Image-based monte carlo localisation with omnidirectional images," *Robotics and Autonomous Systems*, vol. 48, no. 1, pp. 17–30, Aug. 2004.

[13] F. Dellaert, W. Burgard, D. Fox, and S. Thrun, "Using the CONDENSATION algorithm for robust, vision-based mobile robot localization," in *Proc. of 1999 IEEE CVPR*, vol. 2, 1999, pp. 588–594.

[14] O. Wulf, D. Lecking, and B. Wagner, "Robust Self-Localization in industrial environments based on 3D ceiling structures," in *Proc. of 2006 IEEE/RSJ IROS*. IEEE, 2006, pp. 1530–1534.

[15] J. Mason, S. Ricco, and R. Parr, "Textured occupancy grids for monocular localization without features," in *Proc. of 2011 IEEE ICRA*. IEEE, May 2011, pp. 5800–5806.

[16] R. Maffei, V. A. M. Jorge, V. F. Rey, M. Kolberg, and E. Prestes, "Fast monte carlo localization using spatial density information," in *Proc. of 2015 IEEE ICRA*, May 2015, pp. 6352–6358.

[17] S.-Y. Hwang and J.-B. Song, "Stable monocular SLAM with indistinguishable features on estimated ceiling plane using upward camera," in *Proc. of 2008 IEEE ICCAS*. IEEE, 2008, pp. 704–709.

[18] H. Choi, D. Y. Kim, J. P. Hwang, C.-W. Park, and E. Kim, "Efficient simultaneous localization and mapping based on Ceiling-View: Ceiling boundary feature map approach," *Advanced Robotics*, vol. 26, no. 5-6, pp. 653–671, 2012.

[19] S. Ramalingam, S. Bouaziz, P. Sturm, and M. Brand, "Skyline2gps: Localization in urban canyons using omni-skylines," in *Proc of 2010 IEEE/RSJ IROS*, Oct 2010, pp. 3816–3823.

[20] H. Moravec and A. Elfes, "High resolution maps from wide angle sonar," in *Proc. of 1985 IEEE ICRA*. IEEE, 1985, pp. 116–121.